Archives of Biochemistry and Biophysics 729 (2022) 109392

Contents lists available at ScienceDirect

Archives of Biochemistry and Biophysics

journal homepage: www.elsevier.com/locate/yabbi

Different phenotypic outcome due to site-specific phosphorylation in the cancer-associated NQO1 enzyme studied by phosphomimetic mutations

Juan Luis Pacheco-Garcia [a], Ernesto Anoz-Carbonell [b], Dmitry S. Loginov [c], Pavla Vankova [d], Eduardo Salido [e], Petr Man [c], Milagros Medina [b], Rogelio Palomino-Morales [f], Angel L. Pey [g,*]

[a] Departamento de Química Física, Universidad de Granada, Av. Fuentenueva s/n, 18071, Granada, Spain
[b] Departamento de Bioquímica y Biología Molecular y Cellular, Facultad de Ciencias, Instituto de Biocomputación y Física de Sistemas Complejos (BIFI) (GBsC-CSIC Joint Unit), Universidad de Zaragoza, 50009, Zaragoza, Spain
[c] Institute of Microbiology - BioCeV, Academy of Sciences of the Czech Republic, Prumyslova 595, Vestec, 252 50, Czech Republic
[d] Institute of Biotechnology - BioCeV, Academy of Sciences of the Czech Republic, Prumyslova 595, Vestec, 252 50, Czech Republic
[e] Center for Rare Diseases (CIBERER), Hospital Universitario de Canarias, Universidad de la Laguna, 38320, Tenerife, Spain
[f] Department of Biochemistry and Molecular Biology I, Faculty of Sciences and Biomedical Research Center (CIBM), University of Granada, Granada, Spain
[g] Departamento de Química Física, Unidad de Excelencia en Química Aplicada a Biomedicina y Medioambiente e Instituto de Biotecnología, Universidad de Granada, Av. Fuentenueva s/n, 18071, Granada, Spain

ARTICLE INFO

Keywords:
Flavoprotein
Phosphorylation
Structure-function relationships

ABSTRACT

Protein phosphorylation is a common phenomenon in human flavoproteins although the functional consequences of this site-specific modification are largely unknown. Here, we evaluated the effects of site-specific phosphorylation (using phosphomimetic mutations at sites S40, S82 and T128) on multiple functional aspects as well as in the structural stability of the antioxidant and disease-associated human flavoprotein NQO1 using biophysical and biochemical methods. *In vitro* biophysical studies revealed effects of phosphorylation at different sites such as decreased binding affinity for FAD and structural stability of its binding site (S82), conformational stability (S40 and S82) and reduced catalytic efficiency and functional cooperativity (T128). Local stability measurements by H/D exchange in different ligation states provided structural insight into these effects. Transfection of eukaryotic cells showed that phosphorylation at sites S40 and S82 may reduce steady-levels of NQO1 protein by enhanced proteasome-induced degradation. We show that site-specific phosphorylation of human NQO1 may cause pleiotropic and counterintuitive effects on this multifunctional protein with potential implications for its relationships with human disease. Our approach allows to establish relationships between site-specific phosphorylation, functional and structural stability effects *in vitro* and inside cells paving the way for more detailed analyses of phosphorylation at the flavoproteome scale.

1. Introduction

Human NAD(P)H:quinone oxidoreductase 1 (NQO1) is a multifunctional protein whose dysregulation has been associated with developing cancer, Alzheimer's and Parkinson's disease [1–3]. It catalyzes the two-electron reduction of a wide variety of quinones, including maintenance of vitamins in their reduced state, superoxide scavenging, detoxification of xenobiotics and activation of cancer pro-drugs [1,3–5]. Additionally, NQO1 interacts with other proteins (PPI, e.g. p53 and HIF-1) and with RNA molecules [1,6–9].

NQO1 forms dimers with two active sites, each of them containing a tightly bound FAD molecule required for catalysis and also providing intracellular stability [10–13]. The monomer contains two domains: an N-terminal domain (NTD; residues 1–225) containing the FAD binding site and most of the monomer:monomer interface (MMI), whereas the C-terminal domain (CTD, residues 226–274) completes the active sites [11–15].

NQO1 displays a remarkable functional chemistry. During its catalytic cycle, two half-reactions occur: i) in the reductive half-reaction the FAD molecules are reduced upon NAD(P)H binding and hydride transfer (HT), which constitutes the rate-limiting step of the catalytic cycle; ii) in the oxidative half-reaction, upon release of $NAD(P)^+$, the substrate binds and is reduced by $FADH_2$ reconstituting the holo-enzyme [15,16]. Enzyme kinetic analyses have supported the existence of non-equivalent active sites that yield negative cooperativity to this catalytic cycle

* Corresponding author.
E-mail address: angelpey@ugr.es (A.L. Pey).

https://doi.org/10.1016/j.abb.2022.109392
Received 10 August 2022; Received in revised form 29 August 2022; Accepted 31 August 2022
Available online 9 September 2022

Abbreviations

BB	binding buffer
CTD	C-terminal domain
DBS	dicoumarol binding site;
Dic	dicoumarol
DT	deuteride-transfer
FAD	flavin-adenine dinucleotide;
$FADH_2$	reduced flavin-adenine dinucleotide;
FBS	FAD binding site;
HDX	hydrogen-deuterium exchange
HT	hydride-transfer
IMAC	immobilized-metal affinity chromatography
KIE	kinetic isotope effect
LB	Luria-Bertani
MMI	monomer:monomer interface
NQO1	NAD(P)H:quinone oxidoreductase 1
$NQO1_{apo}$	ligand-free NQO1
$NQO1_{holo}$	NQO1 with FAD bound
NTD	N-terminal domain
PPI	protein:protein interactions
SEC	size-exclusion chromatography
SDS-PAGE	polyacrylamide gel electrophoresis in the presence of sodium dodecylsulphate
TCEP	Tris(2-carboxyethyl)phosphine hydrochloride;
TCS	thermolysin cleavage site.

[16–18].

In addition, ligands bound to NQO1 modulate its multiple functions. In the FAD-free state ($NQO1_{apo}$), the enzyme is inactive, intracellularly unstable and displays altered PPI [10,19]. FAD binding renders a conformational state ($NQO1_{holo}$), ready to initiate catalysis, intracellularly stable and with a different interactomic pattern than that of $NQO1_{apo}$ [10,19]. Upon NAD(P)H binding, the FAD is reduced to $FADH_2$ constituting a catalytically relevant state that also shuttles the proteins to interact with microtubules and enhances PPI [6,16,20]. Binding of dicoumarol (Dic), a competitive inhibitor of both NAD(P)H and the substrate [16], leads to an inactive state likely reflecting the ternary complex (NQO1holo:NAD(P)H) or transition state analogue, also abrogating PPI [6]. It is interesting to note that we have recently characterized the effects of FAD and Dic binding to WT NQO1, revealing that ligand binding sequentially stabilizes the FAD (FBS) and Dic (DBS) binding sites, and these stabilizing effects propagate far beyond these sites affecting the entire structure of the enzyme [21].

Phosphorylation is a common phenomenon in human flavoproteins, although the functional consequences of these events are largely unknown (https://www.phosphosite.org/). By July 30, 2022, there were 12 phosphorylation events identified in human NQO1 based on high-throughput approaches (Fig. 1A). Most of them are localized in the NTD (Fig. 1A). Three of these sites (S40, S82 and T128) have been characterized in some detail at the molecular level by phosphomimetic mutations or by direct phosphorylation [2,18,22,23](Fig. 1B). The phosphomimetic mutation S82D affects a partially solvent exposed residue far from the FBS and the DBS (at minimal distances of 14 Å and 18.5 Å, respectively)(Fig. 1B). S82D causes local destabilization of the structure, and this effect propagates to the FBS and reduces by ~10-fold the affinity for the cofactor and thus its intracellular stability likely due to increased population of the $NQO1_{apo}$ state [22]. In addition, S82D decreases the catalytic efficiency for the slow FAD reduction pathway, thus exacerbating the functional negative cooperativity displayed by WT NQO1 [18]. The kinase responsible for phosphorylation of S82 is unknown. S40 is fully buried in the crystal structure and also locates far from the FBS and DBS (minimal distances of 14.5 Å and 20 Å, respectively). T128 is a solvent exposed residue that locates closer to the DBS (minimal distance of 6.8 Å) and at 12 Å from the FBS (Fig. 1B). Importantly, it is next to Y129, that undergoes important conformational rearrangements upon Dic binding [24]. S40 and T128 sites are both phosphorylated by the Akt kinase, although phosphorylation of the T128 site seems to be important to trigger phosphorylation at both sites [2]. Phosphorylation at S40 and T128 may facilitate ubiquitination and degradation of NQO1, with a more important role of phosphorylation at T128 [2]. This decrease in intracellular stability due to phosphorylation at S40/T128 may lower the antioxidant and cytoprotective capacity of NQO1 in cultured cells [2]. This study has also associated phosphorylation of T128 with increased propensity to develop Parkinson's disease [2].

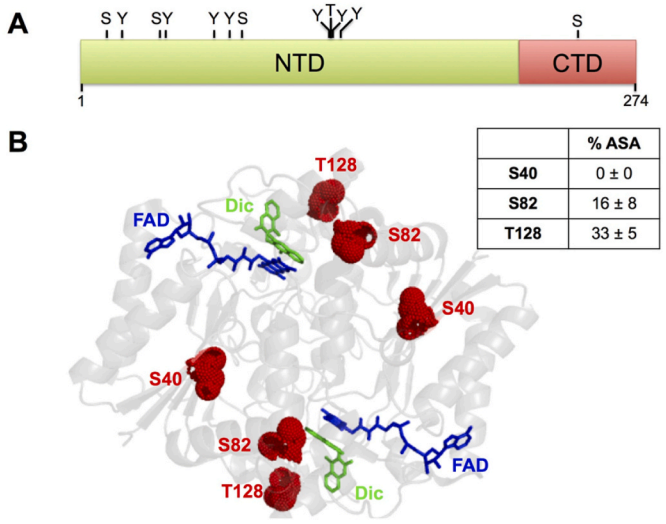

Fig. 1. Phosphorylation sites in human NQO1. A) Schematic representation of the different phosphorylation sites in the primary sequence of NQO1 (as described in Phosphosite Plus®; https://www.phosphosite.org/); B) Structural location of the phosphorylation sites at S40, S82 and T128 investigated in this work (PDB code 2F1O) [24]. The percentage of accessible surface area (% ASA) was determined usin GetArea (http://curie.utmb.edu/getarea.html) [34] and it is reported as the average ± s.d. from eight monomers found in this crystallographic structure.

Overall, these studies suggest that phosphorylation of NQO1 at different sites (S40, S82 and T128) may impair the stability of the enzyme inside cells. However, the structural and functional consequences of these phosphorylation events individually on the multifunctional NQO1 are not well known. In this work, we have carried out a comparative and multidisciplinary structure-function analysis of these phosphorylation events using *phosphomimetic* mutations (S40D, S82D ad T128D) and *unphosphorylatable* variants (S40A, S82A and T128A).

2. Materials and methods

2.1. Protein expression and purification

Mutations were introduced by site-directed mutagenesis on the wild-type (WT) NQO1 cDNA cloned into the pET-15b vector (pET-15b-NQO1) by GenScript (Leiden, The Netherlands). Codons were optimized for expression in *E. coli* and mutagenesis was confirmed by sequencing.

Typically, 40 mL of Luria-Bertani (LB) medium containing 0.1 mg mL^{-1} ampicillin (Canvax Biotech, Córdoba, Spain) were inoculated with transformed cells and grown for 16 h at 37 °C. These cultures were diluted into 800 mL of LB containing 0.1 mg mL^{-1} ampicillin, grown at

37 °C for 3 h to reach an optical density of about 1.0 and then these were transferred to 25 °C and induced with 0.5 mM IPTG (Isopropyl β-*d*-1-thiogalactopyranoside, Canvax Biotech). After 6 h, cells were harvested by centrifugation and frozen at −80 °C for 16 h. Cells were resuspended in binding buffer, BB (20 mM Na-phosphate, 300 mM NaCl, 50 mM imidazole, pH 7.4) with 1 mM PMSF (phenylmethylsulfonyl fluoride, Sigma-Aldrich, Madrid, Spain), sonicated in an ice bath, and the extracts were centrifuged (21000 g, 30 min, 4 °C). Supernatants were loaded into IMAC (immobilized-metal affinity chromatography) columns (Ni-Sepharose, Cytiva, Barcelona, Spain), washed with 30 vol of BB and eluted in this buffer containing 500 mM imidazole. These eluates were buffer exchanged using PD-10 columns (Cytiva, Barcelona, Spain) to 50 mM HEPES-KOH, pH 7.4 and stored at −80 °C. 5–10 mg of protein from IMAC were thawed, centrifuged for 10 min at 21000 g and 4 °C and loaded into a HiLoad® 16/60 Superdex® 200 pg (Cytiva, Barcelona, Spain). Size-exclusion chromatography (SEC) was carried out using 20 mM HEPES-NaOH, 200 mM NaCl, pH 7.4 at 20 °C and at a 1.5 mL min^{-1} flow rate as described [16]. Fractions containing dimeric NQO1 were concentrated and exchanged to HEPES-KOH 50 mM, pH 7.4 using PD-10 columns. After centrifugation for 20 min at 21000 g at 4 °C, the amount of protein (in NQO1 subunit) and the FAD content was determined from the UV–visible spectrum using: $\varepsilon_{(280)} = 47900\ M^{-1}\ cm^{-1}$ for NQO1 and $\varepsilon_{(450)} = 11300\ M^{-1}\ cm^{-1}$ for FAD [25]. Spectra were collected in a Cary 50 spectrophotometer (Agilent Technologies, Waldbronn, Germany) using 0.3 cm path-length quartz cuvettes and ~30 μM of NQO1 in protein subunit. Each NQO1 variant was expressed and analyzed at least three times to check for reproducibility. The purity of NQO1 proteins was evaluated by SDS-PAGE in 12% acrylamide gels (Fig. S1). To obtain apo-proteins, FAD was removed by treatment with 2 M KBr and 2 M urea, 1 mM β-mercapto-ethanol in BB and 1 mM PMSF as previously described [14,25]. Apo-proteins were buffer-exchanged to 50 mM HEPES-KOH, pH 7.4 and contained <3% of FAD bound based on UV–visible spectra. All purified proteins were stored at −80 °C upon flash-freezing in N_2. For enzyme kinetic studies, purified proteins were mixed with a 1 mM FAD solution in 50 mM HEPES-KOH, pH 7.4 for 10 min at room temperature, and the excess of FAD was removed using PD-10 columns. In all cases, this procedure yielded NQO1 protein with more than 95% FAD bound per NQO1 monomer based on UV–visible spectroscopy.

2.2. Titrations with FAD

Fluorescence titrations were carried out at 25 °C using 1 × 0.3 cm path-length cuvettes in a Cary Eclipse spectrofluorimeter (Agilent Technologies). Experiments were carried out in 20 mM sodium phosphate, pH 7.4. 20 μL of a 12.5 μM NQO1 stock solution (in NQO1 subunit) was mixed with 0–500 μL of FAD 10 μM and completed with buffer up to a 1 mL volume. Samples were incubated at 25 °C in the darkness for at least 10 min before measurements. Fluorescence spectra were acquired in the 340–360 nm range upon excitation at 280 nm (slits 5 nm) and spectra averaged over 10 scans using a scan rate of 200 nm min^{-1}. Blanks were also measured similarly (containing only buffer) and subtracted. The intensity of the fluorescence at 350 nm (I) vs. total concentration of FAD ([FAD]) was used to determine the apparent dissociation constant $K_{d(FAD)}$ using equation (1):

$$I = I_{apo} + (I_{holo} - I_{apo}) \cdot \left(\frac{[NQO1] + [FAD] + K_{d(FAD)} - \sqrt{([NQO1] + [FAD] + K_{d(FAD)})^2 - 4 \cdot [NQO1] \cdot [FAD]}}{2 \cdot [NQO1]} \right) \quad \text{Equation 1}$$

where I_{holo} and I_{apo} are the fluorescence intensities of $NQO1_{holo}$ and $NQO1_{apo}$, respectively, and [NQO1] is the total protein concentration (250 nM). This model assumes that FAD binding sites in the NQO1 dimer are equivalent. Data from at least two independent titrations using different preparations of apo-proteins for each NQO1 were used for fittings. The apparent change in binding free energy, $\Delta G_{(FAD)}$, was determined using the following equation: $\Delta G_{(FAD)} = R \cdot T \cdot \ln K_{d(FAD)}$, where R is the ideal gas constant (1.987 cal $mol^{-1}\ K^{-1}$) and T is the absolute temperature (298.15 K) The associated error was determined by linear propagation from the errors of $K_{d(FAD)}$.

2.3. Partial proteolysis with thermolysin

Thermolysin from *Geobacillus stearothermophilus* (Sigma-Aldrich) was prepared in 50 mM HEPES-KOH, pH 7.4 with 100 mM $CaCl_2$. The concentration of thermolysin stock solutions was determined spectrophotometrically using $\varepsilon_{280} = 66086\ M^{-1}\ cm^{-1}$. For proteolysis experiments, purified NQO1 proteins were prepared at ~15 μM NQO1 with 100 μM FAD or 100 μM FAD +100 μM Dic in 50 mM HEPES-KOH, pH 7.4 (all concentrations were final concentrations). Solutions were incubated for 5 min at 25 °C, and reactions were initiated by addition of thermolysin (to 0.1–0.5 μM, final concentration of 10 mM $CaCl_2$). Aliquots were withdrawn at different times, mixed with 25 mM EDTA (ethylenediaminetetraacetic acid), pH 8.0 as final concentration, Laemmli's buffer was added in a 1:1 vol ratio and final solutions were denatured at 95 °C for 5 min. Controls without thermolysin were prepared similarly as samples for time zero. Samples were resolved in SDS-PAGE gels (12% in acrylamide), scanned and analyzed by densitometry using ImageJ (http://rsb.info.nih. gov/ij/). Time-dependent degradation of the full-length protein was fitted using a single exponential function to yield the first-order kinetic constant k_{obs}. The second-order rate constant k_{prot} was determined from k_{obs}/[Thermolysin]. Changes in the local stability (of native vs. cleavable state) upon mutation $\Delta\Delta G_{prot(mut\text{-}WT)}$ were determined by equation (2) [26]:

$$\Delta\Delta G_{prot(WT-mut)} = R \cdot T \cdot ln \frac{k_{prot(mut)}}{k_{prot(WT)}} \quad \text{Equation 2}$$

where R is the ideal gas constant, T is the absolute temperature (298.15 K) and $k_{prot(mut)}$ and $k_{prot(WT)}$ are the second-order rate constants for the mutant and the WT protein, respectively. Errors in $\Delta\Delta G_{prot(WT\text{-}mut)}$ were determined by linear propagation of the fitting errors from the k_{prot} values.

2.4. Thermal denaturation of NQO1 enzymes

Purified NQO1 proteins were prepared at a 2 μM final concentration in subunit in the presence 20 μM of FAD in 50 mM HEPES-KOH, pH 7.4. Samples were loaded into 3 × 3 mm path length quartz cuvettes. Thermal denaturation was carried out in a Cary Eclipse (Varian) spectrofluorimeter equipped with a Peltier element. Samples were equilibrated at 20 °C for 3 min and temperature was increased up to 70 °C at a 2 °C min^{-1} scan rate. Fluorescence emission was recorded at 350 nm (slit 10 nm) upon excitation at 280 nm (slit 5 nm). Experimental curves were normalized using pre- and post-transition linear baselines to provide the apparent half-denaturation temperatures (T_m). For each variant, 3–6 replicas were prepared and analyzed and T_m values were presented as

mean ± s.d. for each variant.

2.5. Hydrogen-deuterium exchange (HDX) monitored by mass spectrometry

Backbone amide hydrogen/deuterium exchange (HDX) was monitored using mass spectrometry as $NQO1_{apo}$ and $NQO1_{holo}$ forms for WT, S40D, S82D and T128D NQO1 variants, and also as $NQO1_{dic}$ for WT and T128D. All procedures including sample preparation, sample measurement and data processing were performed almost identically as described previously [21]. Initial sample concentration was 20 μM and in case of holo-proteins, FAD was included at 200 μM concentration. Dic state was prepared from the holo-form by adding dicoumarol to final concentration of 200 μM. After a 10 min incubation at 25 °C, H/D exchange reaction was initiated by a 10-fold dilution of the protein solution into D_2O-based 50 mM HEPES-KOH, pD 7.4, 1 mM TCEP (tris (2-carboxyethyl)phosphine). Exchange was thus performed at 2 μM protein concentration. Aliquots were taken at 10 s, 30 s, 2 min, 5 min, 20 min, 1 h and 3 h and time points 10 s, 5 m, 3 h were replicated. The reaction was quenched by the addition of 0.5 M Glycine-HCl, pH 2.3 in a 1:1 ratio and flash frozen in liquid N_2. LC-MS analysis was started by rapid thawing of the sample and injection onto the custom-made coimmobilized nepenthesin-2 (Nep2) and pepsin column. Generated peptides were trapped and desalted on a SecurityGuard™ pre-column (ULTRA Cartridges UHPLC Fully Porous Polar C18, 2.1 mm, Phenomenex, Torrance, CA, USA). The digestion and desalting were driven by 0.4% formic acid (FA) in water pumped by 1260 Infinity II Quaternary pump (Agilent Technologies, Waldbronn, Germany) at a flow rate of 200 μL min^{-1}. Desalted peptides were then separated on an analytical column (LUNA® Omega Polar C18 Column, 100 Å, 1.6 μm, 100 mm × 1.0 mm, Phenomenex, Torrance, CA, USA) using a linear gradient (10–45% B in 7 min) followed by a quick step to 99% B lasting 5 min, where the solvent A was 0.1% FA/2% acetonitrile (ACN) in water, B was 0.1% FA/98% ACN in water. The gradient was delivered by the 1290 Infinity II LC System (Agilent Technologies, Waldbronn, Germany) at a flow rate 40 μL min^{-1}. The analytical column was coupled to an ESI source of 15T FT-ICR mass spectrometer (Solarix XR, Bruker Daltonics, Bremen, Germany) operating in broad-band MS mode. Acquired data were exported using DataAnalysis v. 5.3 (Bruker Daltonics, Bremen, Germany), processed by in-house designed software called DeutEx and handled as described previously [21]. Peptide identification was performed using separate LC-MS/MS analyses employing the same UPLC system and settings but coupled to a timsTOF Pro PASEF instrument (Bruker Daltonics, Bremen, Germany). Data were searched by MASCOT (version 2.4, Matrix Science, London, United Kingdom) against a custom-built database containing sequences of the proteases, NQO1 variants and common contaminations as listed in the cRAP databse. Decoy search was enabled, false-discovery ratio was set to 1% and ion score cut-off to 20. Fully deuterated proteins were prepared as described previously [21] and correction for back-exchange was applied according to Ref. [27]. HDX results are presented as $\Delta\%D_{av}$, a parameter that compares a given segment between two variants in a given ligation state (i.e. $S40D_{apo}$ vs. WT_{apo}) as the average of the three time points that show maximal difference in percentage of incorporated deuterium (% D) along a time course [21].

The HDX-MS data have been deposited to the ProteomeXchange Consortium via the PRIDE [28] partner repository with the dataset identifier PXD034600.

2.6. Pre-steady state enzyme kinetic analysis

Hydride-(HT) or deuteride-(DT) transfer reactions from NADH/D to NQO1 were carried out under anaerobic conditions using a stopped-flow spectrophotometer (SX.18 MV, Applied Photophysics Ltd., Leatherhead, UK) interfaced with a photodiode array detector, essentially as described [16]. Reactions were performed in 20 mM HEPES-KOH, pH 7.4. The reductive half-reaction was measured by mixing $NQO1_{holo}$ variants (7.5 μM) with NADH ranging from 7.5 to 100 μM. Multiple wavelength absorption data in the flavin absorption region were collected and processed as described [16]. Time-dependent spectral deconvolution was performed by global analysis and numerical integration methods using previously described procedures [16]. Deconvolution was carried out considering sequential and irreversible steps in the context of two (A→B→C) or three (A→B→C→D) step mechanisms, were A-D are spectral species, and allowed to determine observed rate constants (k_{obs}) for these steps as well as spectroscopic properties of intermediate A to D species. According to a recent study, catalytically relevant processes involved steps A→B (*Fast*) and B→C (*Slow*) [16]. Hyperbolic dependences of k_{obs} vs. NADH concentrations were fitted using equation (3):

$$k_{obs} = \frac{k_{HT} \cdot [NADH]}{K_{d(NADH)} + [NADH]} \quad \text{Equation 3}$$

where k_{HT} is the limiting rate constant for HT and $K_{d(NADH)}$ is the equilibrium dissociation constant to a given active site.

Primary KIEs in the HT process were estimated as previously reported [16] in samples containing equimolar mixtures (7.5 μM of each component) by evaluating HT or DT k_{obs} (k_{obsHT} or k_{obsDT}) from NADH and [4R-^{2}H]-NADD to $NQO1_{ox}$ at different temperatures in the 6–20 °C range. Estimation of the activation parameters (frequency factor, A, and the activation energy, E_a) were determined using the Arrhenius equation as described [16].

2.7. Expression analyses in eukaryotic cells

Site-directed mutagenesis to S40A, S40D, S82A, S82D, T128A or T128D was carried out on the wild-type (WT) NQO1 cDNA cloned into the pCI-NEO plasmid by GenScript (Leiden, The Netherlands). Mutagenesis was confirmed by sequencing the entire cDNA.

HAP1 NQO1 knockout cells (HAP1 NQO1-KO; Horizon, Waterbeach, UK) were cultured in Iscove's modified Dulbecco's medium (IMDM, Lonza, Barcelona, Spain) supplemented with 10% fetal bovine serum (HyClone, GE Healthcare, Barcelona, Spain), 100 U mL^{-1} penicillin and 100 μg mL^{-1} streptomycin (Sigma Aldrich, Madrid, Spain) and cultured at 37 °C in a humidified incubator with 5% CO_2. Cells were transfected using Lipofectamine LTX with Plus Reagent (Thermo Fisher Scientific, Madrid, Spain) and selected using 1 mg mL^{-1} of G418 (Sigma Aldrich). For proteasomal inhibition studies, MG-132 (Calbiochem, Merck, Madrid, Spain) was added to the medium at 10 μg mL^{-1} for 6 h at 37 °C. After treatment with or without MG-132, cells were scrapped and lysed in RIPA buffer (50 mM Tris-HCl, 150 mM NaCl, 0.1% Triton X-100, 0.1% sodium dodecyl sulphate, 1 mM sodium orthovanadate, 1 mM NaF, pH 8.0) with protease inhibitors (COMPLETE, from Roche, Spain). Soluble extracts were denatured using Laemmli's buffer, resolved by SDS-PAGE and transferred to Polyvinylidene difluoride (PVDF) membranes (GE Healthcare). Immunoblotting was carried out using primary monoclonal antibodies anti-NQO1 (sc-393736, Santa Cruz Biotechnology, Dallas, TX, USA) and β-actin (sc-47778, Santa Cruz Biotechnology) from mouse at 1:200 and 1:5000 dilutions, respectively. As a secondary antibody, we used anti-mouse IgG-HRP (sc-516102, Santa Cruz Biotechnology) at 1:2000 dilution. Samples were visualized using luminol-based enhanced chemiluminescence (from BioRad Laboratories, Hercules, CA, USA) and analyzed using Image Lab (from BioRad Laboratories). NQO1 levels were normalized using the levels of β-actin.

3. Results and discussion

3.1. Effect of phosphomimetic mutations on FAD binding

We produced and purified WT, S40A/D, S82A/D and T128A/D variants of human NQO1 (Fig. S1). All variants seemed well-folded, as

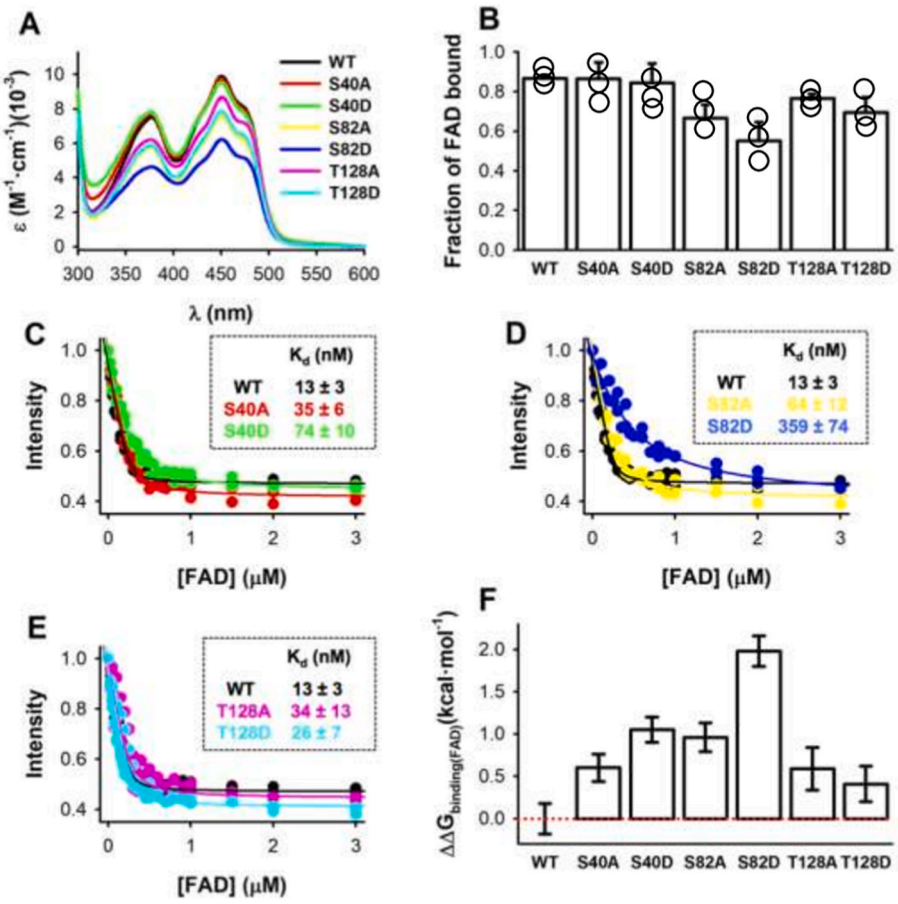

Fig. 2. FAD content and binding affinity. A) UV–vis spectra normalized per NQO1 monomer. B) The fraction of FAD bound determined from the spectra shown in A and considering ε_{450} = 11300 M^{-1} cm^{-1} for NQO1 fully saturated with FAD. Data were the mean ± s.d. from at least three independent purifications of each variant. Experiments in A-B were performed using ~30 μM NQO1 monomer in 50 mM HEPES-KOH pH 7.4. C-E) Titrations of apo-proteins with FAD. K_d values were estimated from simultaneous fitting of data from 2 to 4 indepedent titrations for each variant; Titrations were carried out using 250 nM NQO1 monomer in 20 mM sodium phosphate, pH 7.4 at 25 °C; F) Changes in FAD binding free energy (mutant-WT). Errors are those from linear propagation from those in K_d values.

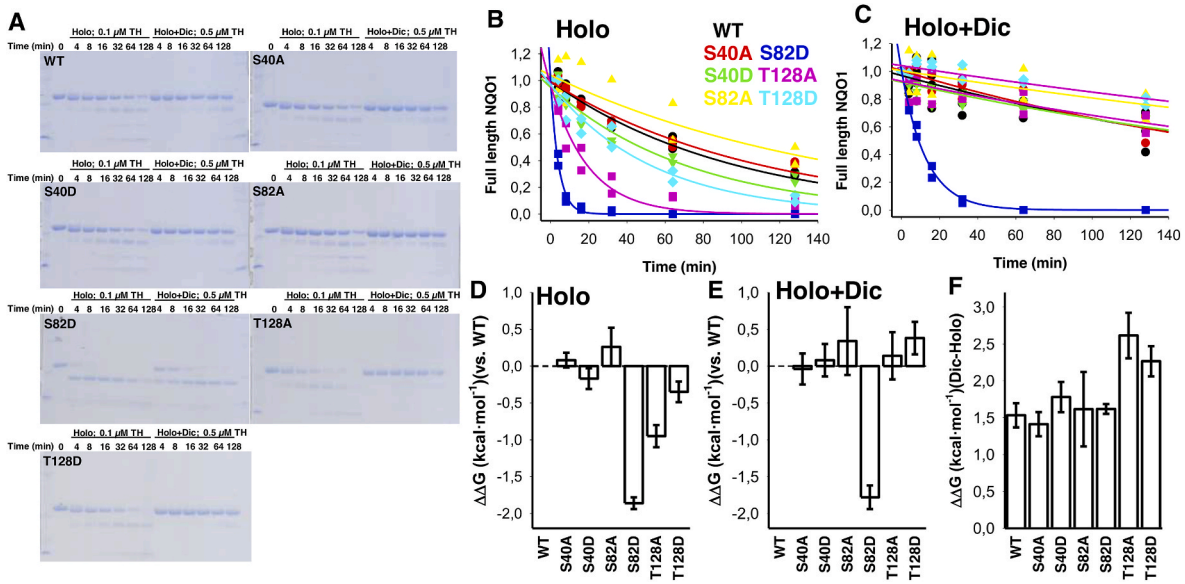

Fig. 3. Stability of the NTD evaluated by partial proteolysis. A) SDS-PAGE analysis of proteolysis kinetics with thermolysin. B–C) Protelysis kinetics of NQO1 proteins. Data are from at least 2 independent experiments for each NQO1 variant. D-E) Effect of different mutation on the thermodynamic stability of the cleavage site vs. WT ($\Delta\Delta G = -R{\cdot}T{\cdot}ln\,\frac{k_{mut}}{k_{WT}}$) as $NQO1_{holo}$ (D) and $NQO1_{dic}$ (E). F) Effect of Dic binding on the thermodynamic stability of the cleavage site for each variant ($\Delta\Delta G = -R{\cdot}T{\cdot}ln\,\frac{k_{dic}}{k_{holo}}$). Experiments were carried out using ~15 μM NQO1 with 100 μM FAD or 100 μM FAD +100 μM Dic in 50 mM HEPES-KOH 10 mM $CaCl_2$, pH 7.4 at 25 °C and the thermolysin concentrations indicated. Errors in panels D–F are those linealy propagated from those of the second-order rate constants k_{prot}.

indicated by size-exclusion chromatography (SEC) and circular dichroism (CD) spectroscopy (Fig. S1). We then carried out" a detailed *in vitro* characterization of their functional properties. First, to test whether phosphomimetic mutations may affect FAD binding affinity, we measured the FAD content in NQO1 protein samples as purified, that qualitatively correlates with FAD binding affinity [25,29–31]. The most noticeable decrease in FAD content was found for S82D, whereas this decrease was milder in T128D (Fig. 2A and B). It must be noted that the mutated sites are not in close proximity to the FAD molecule: the minimal distance from S40 is of 14.5 Å, for S82 is 14 Å and for T128 is 12 Å (using the structure with PDB code 2F1O) [24] that supports long-range propagation of mutational effects to the FBS. To provide quantitative measurements on FAD binding affinity, we then prepared all variants in the $NQO1_{apo}$ state and carried out titrations with FAD monitored by fluorescence spectroscopy (Fig. 2C–F). The mutant S82D showed the largest effect, with a ~30-fold decrease in binding affinity (~2.0 kcal mol^{-1} in binding free energy), whereas the effects of S40D and T128D were milder (6-fold and 2-fold, corresponding to changes in binding free energy of ~1.1 kcal mol^{-1} and ~0.4 kcal mol^{-1}, respectively). These results highlight that the proximity of the phosphorylation site to the FBS or the solvent accessibility of the phosphorylated site does not solely determine their impact on FAD binding affinity. Since FAD binding affinity and intracellular flavin availability may be important for NQO1 intracellular stability [10], these analyses suggest that different phosphomimetic mutations may cause different response to riboflavin supplementation in terms of intracellular stability and activity.

3.2. Effect of the phosphomimetic mutations on the local stability of the NTD

Proteolysis by thermolysin is a useful tool for evaluating the effect of mutations and ligand binding on the thermodynamic local stability of the NTD, in particular due to initial cleavage between S72–V73 (the thermolysin cleavage site, TCS) [13]. Among the phosphomimetic mutants investigated, the most noticeable effect was found for S82D that destabilized by 2 kcal mol^{-1} both in the $NQO1_{holo}$ and $NQO1_{dic}$ states (Fig. 3). The effects of S40D and T128D were much weaker, and in the case of T128D, Dic binding essentially abolished the 0.5 kcal mol^{-1} destabilization caused by this mutation in the TCS of the $NQO1_{holo}$ state. Thus, destabilization of the TCS correlated well with the effect of the phosphomimetic mutations on FAD binding affinity on the $NQO1_{holo}$ state. It is interesting to note that the control variant T128A displays larger sensitivity towards proteolysis than T128D in the $NQO1_{holo}$ state, suggesting that at this residue, a decrease in side-chain causes more significant perturbations on the local stability of the NTD than introduction of a negative charge.

3.3. Effects of phosphomimetic mutations on conformational stability

The thermal stability of NQO1 provides information on the stability of the monomers and the MMI in the dimer, since the NQO1 dimers undergoes unfolding and dissociation prior to the rate-limiting step of irreversible denaturation [30]. We thus evaluated the effects of phosphomimetic mutations on the conformational stability as $NQO1_{holo}$ proteins (Fig. 4). The largest effects were observed for the mutations S40D and S82D, that decreased by ~7 °C the thermal stability of the enzyme. It is interesting to note that denaturation of S82D showed a wider profile, possibly affecting the denaturation mechanism (e.g. this mutation may affect the *coupling* between domains in the irreversible denaturation process). Consequently, the S40D and S82D mutations may destabilize the NQO1 monomer and/or the MMI in the dimer.

3.4. Effects of phosphomimetic mutations on the local stability from HDX

Hydrogen-deuterium exchange (HDX) has been proven to provide high-resolution information on the local stability effects on NQO1 due to mutations and ligand binding, including long-range propagation of these effects across the structure [18,21]. Since the EX1 regime was marginally detected (Fig. S2), it is reasonable to interpret our HDX data using a local thermodynamic stability approach (i.e. EX2) and, in this context, little information on protein dynamics can be inferred.

Despite their different solvent accessibilities (% ASA; S40 < S82 < T128), the impact of phosphomimetic mutations on the local stability of the protein, as determined by HDX, did not correlate with this feature and was strongly dependent on the ligation state (Fig. 5). The S40D mutant showed weak local destabilizing effects based on a EX2 mechanism, and also mildly affected residues of the CTD in the $NQO1_{apo}$ state (Figs. S2 and S3). HDX analyses also allow to suggest that, despite their solvent-accessibility in the crystal structure, these residues are exposed to the solvent (i.e. accessible for phosphorylation) due to local thermodynamic fluctuations (Fig. S2).

In the $NQO1_{apo}$ state, the destabilizing effects of S40D localized in the vicinity of the mutated residue and the CTD, whereas FAD binding restricted these effects to the local environment of S40 (Fig. 5A and Figs. S3–S4). The effects of S82D extended to almost the entire structure of $NQO1_{apo}$ and were of mild-to-moderate intensity (Fig. 5B and Figs. S3–S4). FAD binding restricted these destabilizing effects more locally around the mutated site. The effects of the T128D mutation were very local, destabilizing residues comprising 69–76, while stabilizing residues 126–131 in both the $NQO1_{apo}$ and $NQO1_{holo}$ states (Fig. 5C and Figs. S3–S4).

We then used our HDX studies to investigate different functional sites, namely the residues involved in FAD binding (i.e. the FBS, with implications for FAD binding affinity)(Fig. 6A), solvent-exposed residues (that could be involved in PPI)(Fig. 6B) and the MMI (whose stability is associated with the thermal stability of the enzyme)(Fig. 6C).

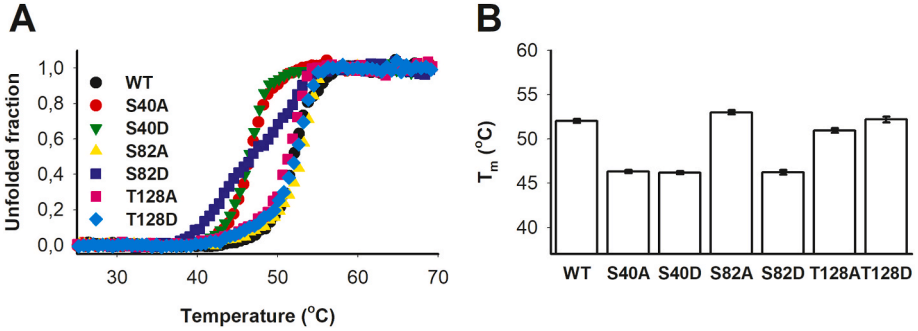

Fig. 4. Thermal stability of NQO1 variants. A) Thermal denaturation profiles of $NQO1_{holo}$ variants as monitored by fluorescence spectroscopy. B) Half-denaturation temperatures (T_m) from at least three different technical replicas (mean ± s.d.). Experiments were carried out using 2 μM NQO1 in the presence 20 μM of FAD in 50 mM HEPES-KOH, pH 7.4 and using a scan rate of 2 °C min^{-1}.

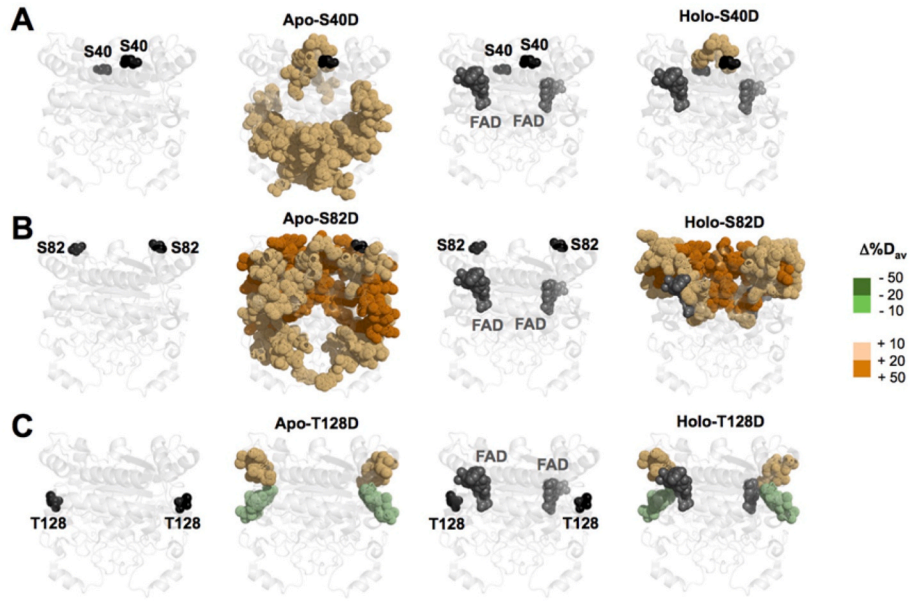

Fig. 5. Overall effects of phosphomimetic mutations on the local stability by HDXMS. A-C) Effect of the mutations S40D (A), S82D (B) and T128D (C) on the local stability of the $NQO1_{apo}$ and $NQO1_{holo}$ states. Changes in stability (as $\Delta\%D_{av}$ using the WT protein in a given ligation state as a reference) are colored according to the scale indicated in the right side of the figure (green tones indicate stabilization whereas orange tones indicate destabilization). Structural display was carried out using the structure with PDB code 2F1O [24]. Experiments were carried out using 20 μM of apo-protein ($NQO1_{apo}$) or purified protein with 200 μM of FAD ($NQO1_{holo}$) and the H/D exchange reaction was initiated by a 10-fold dilution of the protein solution into D_2O-based 50 mM HEPES-KOH, pD 7.4, 1 mM TCEP at 25 °C. (For interpretation of the references to color in this figure legend, the reader is referred to the Web version of this article.)

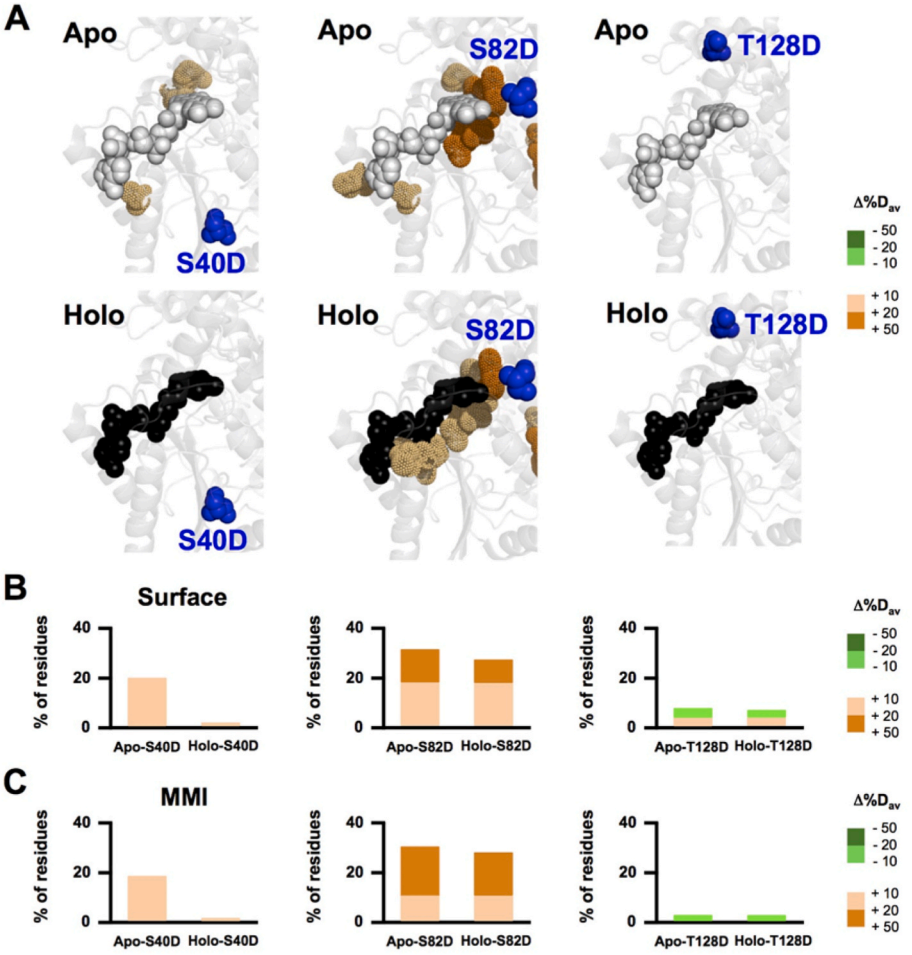

Fig. 6. Effect of phosphomimetic mutations on the local stability of the FBS, protein surface and the MMI. A-C) Effect of the mutations S40D, S82D and T128D mutation on the stability of the FBS in the $NQO1_{apo}$ and $NQO1_{holo}$ states. B) Percentage of residues in the protein surface (considering those with at least 20% solvent accessibility the software GETAREA; http://curie.utmb.edu/getarea.html; (7)); C) Effect of phosphomimetic mutations on the stability of residues belonging to the MMI (considering those determined according to Ref. [21]). Changes in stability (as $\Delta\%D_{av}$ using the WT protein as a reference) are colored according to the scale indicated in the right side of the figure (green tones indicate stabilization whereas orange tones indicate destabilization). Structural display and calculations were carried out using the structure with PDB code 2F1O [24]. Experiments were performed as indicated in the legend of Fig. 5. (For interpretation of the references to color in this figure legend, the reader is referred to the Web version of this article.)

Regarding the stability of the FBS, the mutation S82D caused large changes in stability of the FBS, both in the $NQO1_{apo}$ and $NQO1_{holo}$ states, thus explaining its large effect on FAD binding affinity (Figs. 2 and 6A). The mutation S40D only decreased the stability of small set of residues (A21, Y156 and H162) of the FBS in the $NQO1_{apo}$, thus explaining its milder effect on FAD binding affinity (Figs. 2 and 6A). The lack of noticeable effects of the T128D on the stability of the FBS explains its marginal effect on FAD binding affinity vs. the WT protein (Figs. 2 and

6A).

Residues at the surface of NQO1 may be important for PPI. When we analyzed the effects of the phosphomimetic mutations S40D, S82D and T128D on the stability of solvent-exposed regions of the protein, we also observed different behaviors within the phosphomimetic mutants (Fig. 6B). In the $NQO1_{apo}$ state, the mutation S40D reduced the stability of about 20% of solvent-exposed residues, whereas upon FAD binding, this effect was virtually abolished (Fig. 6B). The mutation S82D affected the stability of about 30% solvent-exposed residues in both the $NQO1_{apo}$ and $NQO1_{holo}$ states (Fig. 6B). The impact of the T128D mutation on solvent-exposed residues was minimal, with mild stabilizing and destabilizing effects (Fig. 6B).

Thermal stability analyses on $NQO1_{holo}$ proteins revealed significant destabilization due to S40D and S82D phosphomimetic mutations (Fig. 4). We then used our HDX studies to determine whether changes in the stability of the MMI correlated with thermal destabilization (Fig. 6C, S5-S6). In the case of S40D, a large destabilization of the MMI is observed in the $NQO1_{apo}$ state. For S82D, the MMI is largely destabilized in both the $NQO1_{apo}$ and $NQO1_{holo}$ states. Changes in the MMI stability were minimal for T128D, consistent with its thermal stability being close to that of the WT protein. Therefore, the large effects of S40D and S82D mutations on thermal stability correlated well with their effect on the stability of the MMI.

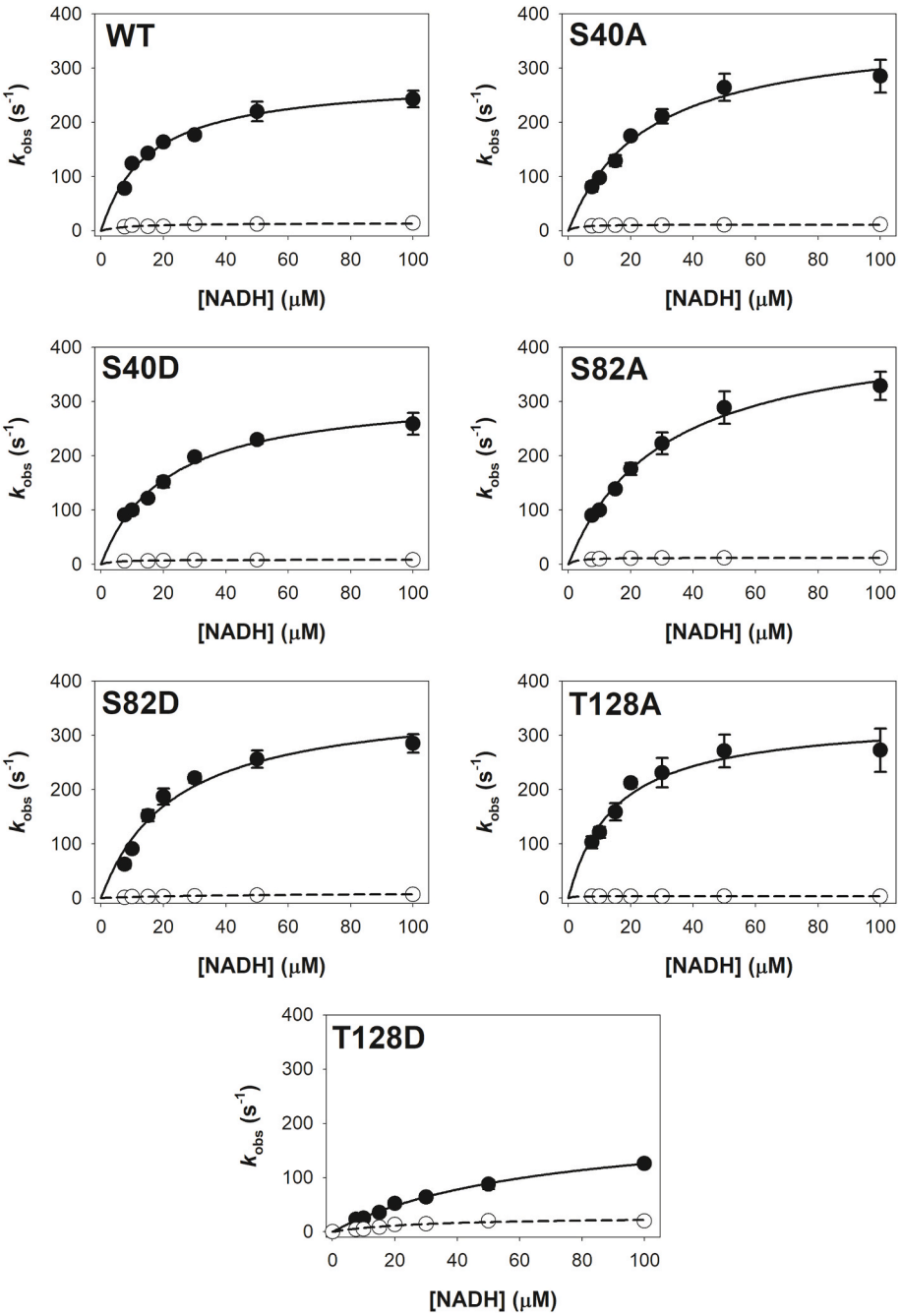

Fig. 7. Effect of phosphomimetic mutations on the reductive half-reaction of FAD using NADH. Data correspond to the fast reduction (closed circles) and slow reduction (open circles) steps and are displayed as mean ± s.d. from three replicates. Lines are fits using equation (3). Fitting parameters are compiled in Table 1. Experiments were carried out using 7.5 μM of $NQO1_{holo}$ in 50 mM HEPES-KOH, pH 7.4 and 6 °C.

Table 1
Kinetic parameters for the NADH-dependent reduction of FAD.

Variant	Fast reduction			Slow reduction		
	k_{HT} (s^{-1})	$K_{d\ (NADH)}$ (μM)	$k_{HT}/K_{d(NADH)}$ ($s^{-1}\cdot\mu M^{-1}$)	k_{HT} (s^{-1})	$K_{d\ (NADH)}$ (μM)	$k_{HT}/K_{d(NADH)}$ ($s^{-1}\cdot\mu M^{-1}$)
WT	281 ± 14	15 ± 2	19 ± 3	14 ± 2	8.2 ± 3.6	1.7 ± 1.0
S40A	372 ± 22	25 ± 4	15 ± 3	12 ± 1	2.3 ± 0.3	5.2 ± 1.1
S40D	320 ± 13	21 ± 2	15 ± 2	8.6 ± 0.3	3.8 ± 0.5	2.3 ± 0.4
S82A	441 ± 19	30 ± 3	15 ± 2	12 ± 1	2.3 ± 0.2	5.2 ± 0.5
S82D	368 ± 33	23 ± 5	16 ± 5	10 ± 1	43 ± 8	0.23 ± 0.06
T128A	333 ± 21	15 ± 3	22 ± 6	3.5 ± 0.1	1.1 ± 0.5	3.2 ± 1.5
T128D	210 ± 12	67 ± 7	3.1 ± 0.5	28 ± 4	29 ± 10	1.0 ± 0.5

3.5. Effects of phosphomimetic mutations on the reductive half-reaction of NQO1

The reduction of the two flavin molecules within the NQO1 dimer occurs through pathways with very different rates (*fast* and *slow* steps) [16]. We have evaluated the effect of phosphomimetic mutations on these two pathways by evaluating rates for HT from NADH by stopped-flow measurements (Fig. 7 and Table 1). Regarding the *fast* pathway of FAD reduction, most of the mutants did not affect significantly the k_{HT} or $K_{d(NADH)}$ values, although the mutation T128D reduced by 4.5-fold the affinity for NADH and by 6-fold the catalytic efficiency (Table 1). In the case of the *slow* reduction pathway, the mutation S82D reduced the affinity for NADH by 5-fold and the catalytic efficiency by 7-fold (Table 1). The mutation T128D increased both the k_{HT} and $K_{d\ (NADH)}$ for the slow step leading to little changes in catalytic efficiency (Table 1). Therefore, the functional cooperativity observed for the WT enzyme is affected differently by the phosphomimetic mutations S82D and T128D (about 4-fold increase and 6-fold decrease, respectively, as the ratio of the catalytic efficiency of the *fast/slow* steps vs. that of WT) (Table 1). It is interesting to note that based on HDX data ($\Delta\%D_{av}$), when we compare the $NQO1_{holo}$ and $NQO1_{dic}$ states of T128D and the WT proteins, some changes in the DBS (but not the FBS) are found for some residues, with different effects on these two states (Pro69 showed decreased stability whereas Tyr127, Tyr129 and Met132 were moderately stabilized)(Figs. S7–S9).

These effects of the mutations S82D and T128D on the enzyme catalytic efficiency for the fast and slow HT steps are likely associated with structural or energetic changes in the active site along the enzyme reaction coordinate. We have recently shown changes in the local stability of the active site (the FBS and DBS) in the $NQO1_{holo}$ and $NQO1_{dic}$ states due to the mutation S82D, particularly destabilization of these functional sites in the former state [18]. Here, we have carried out similar experiments with the mutant T128D (Figs. S7–S9). The mutation T128D affected locally and differently the $NQO1_{holo}$ and $NQO1_{dic}$ states. T128D mildly reduced the stability of a small set of residues in the vicinity of the $NQO1_{holo}$ active site (residues 69–74) whereas its effects were stabilizing, stronger and more extensive in the $NQO1_{dic}$ active site (affecting residues 69–74 and 122–132). A differential analysis of these effects on the local stability of the active site between $NQO1_{dic}$ and $NQO1_{holo}$ clearly showed that the overall effect of the T128D mutation on the active site stability is moderately stabilizing (Fig. S9). Considering that changes in the local stability of the active site between $NQO1_{holo}$ and $NQO1_{dic}$ states might reflect protein stability changes along the reaction coordinate for the HT process [16,18], our results suggest that the mechanisms associated with altered catalytic efficiency of S82D and T128D are different in structural and energetic terms. These results also suggest that site-specific phosphorylation could affect the catalytic efficiency of NQO1 by altering the balance between structural, energetic and dynamic changes along the HT reaction.

To assess the impact of mutations on the dynamics in the active site of NQO1 along its catalytic function, we analyzed HT by using NADH and NADD at different temperatures (Figs. S10–S11). For all variants, *fast* and *slow* reduction steps were slowed down with NADD (Table S1), in general resulting, as reported for the WT, in kinetic isotope effects (KIEs) in the range 1.5–2.2 at the lower temperature evaluated. It is only worth noting a slight increase in KIE for the *fast* process of T128D and the lack of KIE for the *slow* process of T128A. KIEs for the *fast* process are essentially temperature-independent, as for the WT, with the value only slightly decreasing with temperature for S82A (Fig. S11, Table S1). Regarding the *slow* FAD reduction step, only the WT and S40D KIEs were temperature-independent. KIEs particularly decreased with temperature for S40A, S82A and S82D and slightly increased when mutating T128 (Fig. S11). This indicates that mutations hardly alter transitions under the energy barrier and tunnelling of both proton and deuterium in the *fast* HT step, but have a long-distance modulating effect in the *slow* step [16,18]. Analysis of data in the context of Arrhenius theory [activation energies (E_a) and pre-exponential factors (A)] indicated that for the *fast* step of all variants *passive dynamics* is the main source to achieve tunnel ready conformations (Fig. S10). The largest differences were found for *slow* steps. Particularly in S40A, S82A, S82D and T128A that showed remarkable changes in A values (orders of magnitude) and in E_a, *gating* (donor-acceptor-distance sampling) possibly contributes to engage more favourable conformations for a possible tunneling. Thus, replacements at sites S40, S82 and T128 particularly modulate the overall packing and general dynamics of the *slow* active site of NQO1 during HT, and therefore, also contribute to modulate cooperativity in the reductive half-reactions of both active sites in the protein dimer.

3.6. Effects of phosphomimetic mutations on steady-state protein levels upon expression in eukaryotic cells

To evaluate the effect of phosphomimetic mutants on the

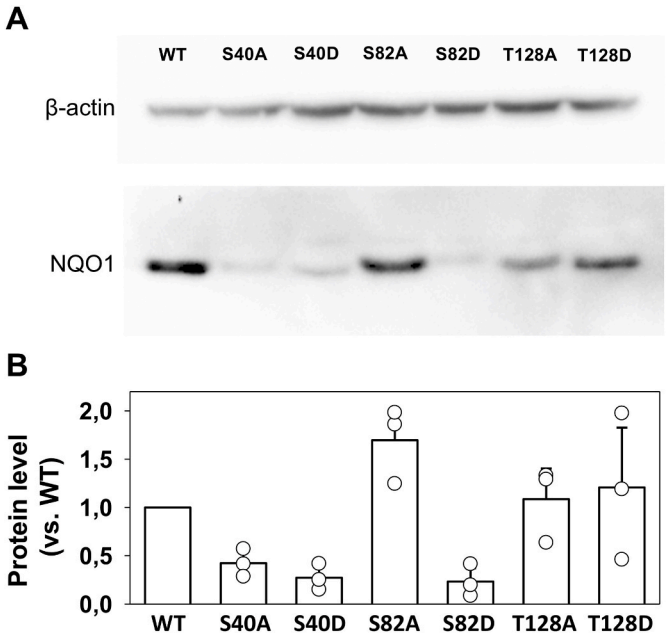

Fig. 8. Effect of phosphomimetic mutations on the NQO1 steady-state protein levels upon expression in stably-transfected HAP-1 KO cells. A) Representative Western-blot analyses; B) Protein levels expressed (considering WT as 1). Data are from three independent transfection experiments (mean ± s.d.) and were normalized by the levels of β-actin.

intracellular protein levels, we transfected HAP-1 KO cells with plasmids encoding WT as well as mutant forms of NQO1 (Fig. 8 and Figs. S12–18). Under these conditions, we considered that steady-state protein levels were determined to some extent by proteasomal degradation of the NQO1 variants (Figs. S12–S15) in agreement with previous studies [2,10,18,32]. The behaviors observed were clearly site-specific. At the S40 site, either S40A or S40D mutants showed lower protein levels (about 30–40% of WT levels), suggesting that even a small perturbation at this site (e.g. S → A) causes significant perturbation of NQO1 intracellular stability. This result suggests that non-conservative mutations S40L and S40W (very rare mutations identified in large-scale sequencing projects of the human genome; i.e. gnomAD database) have dramatic effects on NQO1 intracellular stability. At the S82 site, only the S82D mutant showed decreased protein levels (about 20% of WT), while mutations at the T128 site had little or no effect on protein levels under these conditions. Therefore, our results support that phosphorylation at S40 and S82 sites could lead to reduced protein levels due to accelerated NQO1 degradation.

4. Conclusions

Protein phosphorylation is the most ubiquitous post-translational modification and serves to rapidly modify protein functionality [33]. In the particular case of human flavoproteins, our knowledge on the effects of site-specific phosphorylation is largely unknown [22]. In this work, we have carried out a comparative study of three phosphorylation sites (S40, S82 and T128) in human NQO1, a multifunctional flavoprotein whose dysregulation is associated with cancer and neurological disorders [1,2]. To this end, we used phosphomimetic mutation (S40D, S82D and T128D). These phosphorylation sites display different solvent accessibilities in crystallographic structures, although these solvent accessibilities do not correlate with their impact on the structure, stability and function of NQO1 (Table 2). For instance, the phosphomimetic mutation S40D affects a fully buried serine residue in the protein crystal structure, and causes noticeable effects on *in vitro* and intracellular stability but mild effects on FAD binding affinity. The mutation S82D, affecting a more solvent-exposed residue, affects the conformational and intracellular stabilities, FAD binding and enzyme catalysis of NQO1, and its destabilizing effects propagate more extensively through the protein structure than any of the other sites. The effects of T128D are quite subtle, only causing local stability effects (stabilizing and destabilizing) in the vicinity of the mutated residue that moderately affects enzyme catalysis and cooperativity without a clear effect for the overall *in vitro* or intracellular stability in HAP-1 cells. It is important to realize that our extensive structure-function analyses were carried out using *pseudo-phosphorylating* mutations to isolate the effects of a given individual site. At this point, we realize that a full view of phosphorylation dynamics must include the characterization of a more extended set of phosphorylation sites, the kinases/phosphatase involved, the potential interaction between sites and the parallel or sequential phosphorylation state of different sites [2,22]. We anticipate that our experimental approach will help to improve our knowledge on this challenging task, and would be applied to investigate other human flavoproteins.

CRediT author statement

Juan Luis Pacheco-Garcia.- Data curation, formal analysis, investigation, methodology, resources, validation, visualization, writing – review & editing. **Ernesto Anoz-Carbonell**.- Data curation, formal analysis, investigation, methodology, resources, validation, visualization, writing – review & editing. **Dmitry S. Loginov**.- Data curation, formal analysis, investigation, methodology, resources, validation, visualization, writing – review & editing. **Pavla Vankova**.- Data curation, formal analysis, investigation, methodology, resources, validation, visualization, writing – review & editing. **Eduardo Salido**.- Funding acquisition, resources, writing – review & editing. **Petr Man**.- Data

Table 2
Summary of the effects of phosphomimetic mutations. For each protein variant and feature, these were clustered for semiquantitative comparison in four categories: (++++) mildly improved vs. WT; (+++) WT-like; (++) mildly-moderately impaired vs. WT; (+) largely impaired vs. WT.

Protein feature	NQO1 variant						
	WT	S40A	S40D	S82A	S82D	T128A	T128D
Conformation[a]	+++	+++	+++	+++	+++	+++	+++
FAD bound[b]	+++	+++	+++	++	++	+++	++
FAD binding affinity[c]	+++	+++	++	++	+	+++	+++
Proteolysis Holo[d]	+++	+++	+++	+++	+	++	+++
Proteolysis response to Dic[e]	+++	+++	+++	+++	+++	++++	++++
Thermal stability[f]	+++	+	+	+++	+	+++	+++
Global HDX Apo[g]	+++	N.Det.*	++	N.Det.*	+	N.Det.*	+++
Global HDX Holo[h]	+++	N.Det.*	+++	N.Det.*	+	N.Det.*	+++
FBS HDX[i]	+++	N.Det.*	+++	N.Det.*	+	N.Det.*	+++
MMI HDX[j]	+++	N.Det.*	++	N.Det.*	+	N.Det.*	+++
Fast FAD reduction[k]	+++	+++	+++	+++	+++	+++	+
Slow FAD reduction[l]	+++	++++	++	++++	++	++	++
Cooperativity[m]	+++	++++	+++	++++	+	+++	++
Intracellular abundance[n]	+++	+	+	+++	+	+++	+++

* N. Det.: not determined.
[a] Based on SEC and CD spectroscopy (Fig. S1).
[b] Based on visible absorption spectroscopy (Fig.2A and B).
[c] Based on FAD titrations (Fig. 2C–E).
[d] Based on proteolysis kinetics as holo-proteins (Fig. 3B and D).
[e] Based on the effects of Dic on proteolysis kinetics (Fig. 3D–F).
[f] Based on the effects on thermal stability (Fig. 4).
[g] Based on global HDX for the apo-state (Fig. 5A–C).
[h] Based on global HDX for the **holo**-state (Fig. 5A-C).
[i] Based on HDX results regarding the FBS (Fig. 6A).
[j] Based on HDX results regarding the MMI (Fig. 6C).
[k] Based on the results for the *fast* reduction pathway, including k_{HT}, $K_{d(NADH)}$ and $k_{HT}/K_{d(NADH)}$ (Table 1).
[l] Based on the results for the *slow* reduction pathway, including k_{HT}, $K_{d(NADH)}$ and $k_{HT}/K_{d(NADH)}$ (Table 1).
[m] Based on the results ($k_{HT}/K_{d(NADH)}$) for the *fast/slow* reduction pathways (Table 1).
[n] Based on Western-blot analysis of transfected cells grown without MG-132 (Fig. 8).

curation, formal analysis, funding acquisition, methodology, resources, validation, visualization, software, supervision, writing – review & editing. **Milagros Medina**.- Data curation, formal analysis, funding acquisition, methodology, resources, validation, visualization, software, supervision, writing – review & editing. **Rogelio Palomino-Morales**.- Data curation, formal analysis, methodology, resources, validation, visualization, supervision, writing – review & editing. **Angel L. Pey**.- Conceptualization, Data curation, formal analysis, funding acquisition, investigation, methodology, project administration, resources, validation, visualization, software, supervision, writing - original draft, writing – review & editing.

Funding

JLP-G and ALP were supported by the ERDF/Spanish Ministry of Science, Innovation and Universities—State Research Agency (Grant RTI2018-096246-B-I00), Consejería de Economía, Conocimiento, Empresas y Universidad, Junta de Andalucía (Grant P18-RT-2413) and ERDF/Counseling of Economic transformation, Industry, Knowledge and Universities, Junta de Andalucía (Grant B-BIO-84-UGR20). EA and MM were funded by MCIN/AEI/10.13039/501100011033 (Grant PID2019-103901 GB-I00) and Government of Aragón-FEDER (Grant E35_20R). Financial support from Horizon 2020 EU_FT-ICR_MS project (731077), EU/MEYS projects BioCeV (CZ.1.05/1.1.00/02.0109) and CIISB LM2018127 are acknowledged. Funding for open access charge: Universidad de Granada / CBUA.

Declaration of competing interest

The authors declare no competing, personal financial or other competing interests. Funding or employment sources played no role in the design, presentation or discussion of the presented research.

Data availability

Data will be made available on request.

Acknowledgments

None.

Appendix A. Supplementary data

Supplementary data to this article can be found online at https://doi.org/10.1016/j.abb.2022.109392.

References

[1] S.K. Beaver, N. Mesa-Torres, A.L. Pey, D.J. Timson, NQO1: a target for the treatment of cancer and neurological diseases, and a model to understand loss of function disease mechanisms, Biochim. Biophys. Acta, Proteins Proteomics 1867 (2019) 663–676, https://doi.org/10.1016/j.bbapap.2019.05.002.

[2] S. Luo, S.S. Kang, Z.H. Wang, X. Liu, J.X. Day, Z. Wu, J. Peng, D. Xiang, W. Springer, K. Ye, Akt phosphorylates NQO1 and triggers its degradation, abolishing its antioxidative activities in Parkinson's disease, J. Neurosci. 39 (2019) 7291–7305, https://doi.org/10.1523/JNEUROSCI.0625-19.2019.

[3] D. Ross, D. Siegel, The diverse functionality of NQO1 and its roles in redox control, Redox Biol. 41 (2021), https://doi.org/10.1016/j.redox.2021.101950.

[4] D. Ross, D. Siegel, NQO1 in protection against oxidative stress, Curr. Opin. Toxicol. 7 (2018) 67–72, https://doi.org/10.1016/j.cotox.2017.10.005.

[5] E. Salido, D.J. Timson, I. Betancor-Fernández, R. Palomino-Morales, E. Anoz-Carbonell, J.L. Pacheco-García, M. Medina, A.L. Pey, Targeting HIF-1α function in cancer through the chaperone action of NQO1: implications of genetic diversity of NQO1, J. Personalized Med. 12 (2022) 747, https://doi.org/10.3390/jpm12050747.

[6] G. Asher, P. Tsvetkov, C. Kahana, Y. Shaul, A mechanism of ubiquitin-independent proteasomal degradation of the tumor suppressors p53 and p73, Genes Dev. 19 (2005) 316–321, https://doi.org/10.1101/gad.319905.

[7] G. Ben-Nissan, M. Sharon, Regulating the 20S proteasome ubiquitin-independent degradation pathway, Biomolecules 4 (2014) 862–884, https://doi.org/10.3390/biom4030862.

[8] A. di Francesco, C. di Germanio, A.C. Panda, P. Huynh, R. Peaden, I. Navas-Enamorado, P. Bastian, E. Lehrmann, A. Diaz-Ruiz, D. Ross, D. Siegel, J. L. Martindale, M. Bernier, M. Gorospe, K. Abdelmohsen, R. de Cabo, Novel RNA-binding activity of NQO1 promotes SERPINA1 mRNA translation, Free Radic. Biol. Med. 99 (2016) 225–233, https://doi.org/10.1016/j.freeradbiomed.2016.08.005.

[9] E.T. Oh, J.W. Kim, J.M. Kim, S.J. Kim, J.S. Lee, S.S. Hong, J. Goodwin, R. J. Ruthenborg, M.G. Jung, H.J. Lee, C.H. Lee, E.S. Park, C. Kim, H.J. Park, NQO1 inhibits proteasome-mediated degradation of HIF-1α, Nat. Commun. 7 (2016), 13593 https://doi.org/10.1038/ncomms13593.

[10] A. Martínez-Limón, M. Alriquet, W.H. Lang, G. Calloni, I. Wittig, R.M. Vabulas, Recognition of enzymes lacking bound cofactor by Protein quality control, Proc. Natl. Acad. Sci. U. S. A. 113 (2016) 12156–12161, https://doi.org/10.1073/pnas.1611994113.

[11] M. Faig, M.A. Bianchet, P. Talalay, S. Chen, S. Winski, D. Ross, L.M. Amzel, Structures of recombinant human and mouse NAD(P)H:quinone oxidoreductases: species comparison and structural changes with substrate binding and release, Proc. Natl. Acad. Sci. U. S. A. 97 (2000) 3177–3182, https://doi.org/10.1073/pnas.97.7.3177.

[12] R. Li, M.A. Bianchet, P. Talalayt, L.M. Amzel, The three-dimensional structure of NAD(P)H:quinone reductase, a flavoprotein involved in cancer chemoprotection and chemotherapy: mechanism of the two-electron reduction, Proc. Natl. Acad. Sci. U. S. A. 92 (1995) 8846–8850, https://doi.org/10.1073/pnas.92.19.8846.

[13] E. Medina-Carmona, R.J. Palomino-Morales, J.E. Fuchs, E. Padín-Gonzalez, N. Mesa-Torres, E. Salido, D.J. Timson, A.L. Pey, Conformational dynamics is key to understanding loss-of-function of NQO1 cancer-associated polymorphisms and its correction by pharmacological ligands, Sci. Rep. 6 (2016), 20331, https://doi.org/10.1038/srep20331.

[14] E. Medina-Carmona, J.L. Neira, E. Salido, J.E. Fuchs, R. Palomino-Morales, D. J. Timson, A.L. Pey, Site-to-site interdomain communication may mediate different loss-of-function mechanisms in a cancer-associated NQO1 polymorphism, Sci. Rep. 7 (2017), https://doi.org/10.1038/srep44532.

[15] W.D. Lienhart, V. Gudipati, M.K. Uhl, A. Binter, S.A. Pulido, R. Saf, K. Zangger, K. Gruber, P. Macheroux, Collapse of the native structure caused by a single amino acid exchange in human NAD(P)H:Quinone oxidoreductase, FEBS J. 281 (2014) 4691–4704, https://doi.org/10.1111/febs.12975.

[16] E. Anoz-Carbonell, D.J. Timson, A.L. Pey, M. Medina, The catalytic cycle of the antioxidant and cancer-associated human NQO1 enzyme: hydride transfer, conformational dynamics and functional cooperativity, Antioxidants 9 (2020) 1–22, https://doi.org/10.3390/antiox9090772.

[17] C.F. Megarity, H. Abdel-Aal Bettley, M.C. Caraher, K.A. Scott, R.C. Whitehead, T. A. Jowitt, A. Gutierrez, R.A. Bryce, K.A. Nolan, I.J. Stratford, D.J. Timson, Negative cooperativity in NAD(P)H quinone oxidoreductase 1 (NQO1), Chembiochem 20 (2019) 2841–2849, https://doi.org/10.1002/cbic.201900313.

[18] J.L. Pacheco-Garcia, E. Anoz-Carbonell, P. Vankova, A. Kannan, R. Palomino-Morales, N. Mesa-Torres, E. Salido, P. Man, M. Medina, A.N. Naganathan, A.L. Pey, Structural basis of the pleiotropic and specific phenotypic consequences of missense mutations in the multifunctional NAD(P)H:quinone oxidoreductase 1 and their pharmacological rescue, Redox Biol. 46 (2021), 102112, https://doi.org/10.1016/j.redox.2021.102112.

[19] A. Martínez-Limón, G. Calloni, R. Ernst, R.M. Vabulas, Flavin dependency undermines proteome stability, lipid metabolism and cellular proliferation during vitamin B2 deficiency, Cell Death Dis. 11 (2020) 725, https://doi.org/10.1038/s41419-020-02929-5.

[20] D. Siegel, S. Bersie, P. Harris, A. di Francesco, M. Armstrong, N. Reisdorph, M. Bernier, R. de Cabo, K. Fritz, D. Ross, A redox-mediated conformational change in NQO1 controls binding to microtubules and α-tubulin acetylation, Redox Biol. 39 (2021), 101840, https://doi.org/10.1016/j.redox.2020.101840.

[21] P. Vankova, E. Salido, D.J. Timson, P. Man, A.L. Pey, A dynamic core in human NQO1 controls the functional and stability effects of ligand binding and their communication across the enzyme dimer, Biomolecules 9 (2019) 728, https://doi.org/10.3390/biom9110728.

[22] E. Medina-Carmona, B. Rizzuti, R. Martín-Escolano, J.L. Pacheco-García, N. Mesa-Torres, J.L. Neira, R. Guzzi, A.L. Pey, Phosphorylation compromises FAD binding and intracellular stability of wild-type and cancer-associated NQO1: insights into flavo-proteome stability, Int. J. Biol. Macromol. 125 (2019) 1275–1288, https://doi.org/10.1016/j.ijbiomac.2018.09.108.

[23] J.L. Pacheco-Garcia, D. Loginov, B. Rizzuti, P. Vankova, J.L. Neira, D. Kavan, N. Mesa-Torres, R. Guzzi, P. Man, A.L. Pey, A single evolutionarily divergent mutation determines the different FAD-binding affinities of human and rat NQO1 due to site-specific phosphorylation, FEBS Lett. 596 (2022) 29–41, https://doi.org/10.1002/1873-3468.14238.

[24] G. Asher, O. Dym, P. Tsvetkov, J. Adler, Y. Shaul, The crystal structure of NAD(P)H quinone oxidoreductase 1 in complex with its potent inhibitor dicoumarol, Biochemistry 45 (2006) 6372–6378, https://doi.org/10.1021/bi0600087.

[25] E. Medina-Carmona, J.E. Fuchs, J.A. Gavira, N. Mesa-Torres, J.L. Neira, E. Salido, R. Palomino-Morales, M. Burgos, D.J. Timson, A.L. Pey, Enhanced vulnerability of human proteins towards disease-associated inactivation through divergent evolution, Hum. Mol. Genet. 26 (2017) 3531–3544, https://doi.org/10.1093/hmg/ddx238.

[26] J.E. Fuchs, I.G. Muñoz, D.J. Timson, A.L. Pey, Experimental and computational evidence on conformational fluctuations as a source of catalytic defects in genetic diseases, RSC Adv. 6 (2016) 58604–58612, https://doi.org/10.1039/C6RA05499D.

[27] Z. Zhang, D.L. Smith, Determination of Amide Hydrogen Exchange by Mass Spectrometry: A New Tool for Protein Structure Elucidation, Cambridge University Press, 1993.

[28] Y. Perez-Riverol, J. Bai, C. Bandla, D. García-Seisdedos, S. Hewapathirana, S. Kamatchinathan, D.J. Kundu, A. Prakash, A. Frericks-Zipper, M. Eisenacher, M. Walzer, S. Wang, A. Brazma, J.A. Vizcaíno, The PRIDE database resources in 2022: a hub for mass spectrometry-based proteomics evidences, Nucleic Acids Res. 50 (2022), https://doi.org/10.1093/nar/gkab1038. D543–D552.

[29] A.L. Pey, Biophysical and functional perturbation analyses at cancer-associated P187 and K240 sites of the multifunctional NADP(H):quinone oxidoreductase 1, Int. J. Biol. Macromol. 118 (2018) 1912–1923, https://doi.org/10.1016/j.ijbiomac.2018.07.051.

[30] A.L. Pey, C.F. Megarity, D.J. Timson, FAD binding overcomes defects in activity and stability displayed by cancer-associated variants of human NQO1, Biochim. Biophys. Acta (BBA) - Mol. Basis Dis. (2014) 2163–2173, https://doi.org/10.1016/j.bbadis.2014.08.011, 1842.

[31] J.L. Pacheco-García, M. Cano-Muñoz, I. Sánchez-Ramos, E. Salido, A.L. Pey, Naturally-occurring rare mutations cause mild to catastrophic effects in the multifunctional and cancer-associated NQO1 protein, J. Personalized Med. 10 (2020) 1–31, https://doi.org/10.3390/jpm10040207.

[32] D. Siegel, A. Anwar, S.L. Winski, J.K. Kepa, K.L. Zolman, D. Ross, Rapid polyubiquitination and proteasomal degradation of a mutant form of NAD(P)H: quinone oxidoreductase 1, Mol. Pharmacol. 59 (2001) 263–268.

[33] J.A. Ubersax, J.E. Ferrell Jr., Mechanisms of specificity in protein phosphorylation, Nat. Rev. Mol. Cell Biol. 8 (2007) 530–541, https://doi.org/10.1038/nrm2203.

[34] R. Fraczkiewicz, W. Braun, Exact and efficient analytical calculation of the accessible surface areas and their gradients for macromolecules, J. Comput. Chem. 19 (1998) 319–333. https://doi.org/10.1002/(SICI)1096-987X(199802)19:3<319::AID-JCC6>3.0.CO;2-W. https://doi.org/10.1002/(SICI)1096-987X(199802)19:3%3c319::AID-JCC6%3e3.0.CO;2-W.